

Low-frequency variability of surface air temperature over the Barents Sea: causes and mechanisms

Eveline C. van der Linden¹ · Richard Bintanja¹ · Wilco Hazeleger^{1,2} · Rune G. Graversen³

Received: 8 May 2015 / Accepted: 28 October 2015 / Published online: 19 November 2015
© Springer-Verlag Berlin Heidelberg 2015

Abstract The predominant decadal to multidecadal variability in the Arctic region is a feature that is not yet well-understood. It is shown that the Barents Sea is a key region for Arctic-wide variability. This is an important topic because low-frequency changes in the ocean might lead to large variations in the sea-ice cover, which then cause massive changes in the ocean-atmosphere heat exchanges. Here we describe the mechanism driving surface temperatures and heat fluxes in the Barents Sea based primarily on analyzes of one global coupled climate model. It is found that the ocean drives the low-frequency changes in surface temperature, whereas the atmosphere compensates the oceanic transport anomalies. The seasonal dependence and the role of individual components of the ocean-atmosphere energy budget are analyzed in detail, showing that seasonally-varying climate mechanisms play an important role. Herein, sea ice is governing the seasonal response, by acting as a lid that opens and closes during warm and cold periods, respectively, thereby modulating the surface heat fluxes.

Keywords Barents Sea · Multidecadal variability · Arctic climate · Coupled atmosphere-ocean model

1 Introduction

Large low-frequency climate variations in the Arctic have been detected in observations during the last 100 years

(Polyakov et al. 2003). To distinguish anthropogenically forced temperature trends from decadal to multidecadal natural climate variability, it is important to obtain a better understanding of its many aspects and causes. The difference in simulated and observed trend patterns of Arctic near-surface temperature over land (1900–2008) is larger than would be expected based on the difference between individual model simulations in a multi-model ensemble (Gillett et al. 2008). This indicates that observed changes in Arctic temperature are not consistent with natural temperature variability alone. Decadal to multidecadal climate variability might sometimes enhance and at other times reduce long-term (anthropogenic) trends (Parker et al. 2007). This can also have implications for understanding the recent and early twentieth century warming trends in the Arctic as part of attributing Arctic climate change to human activities.

Arctic temperature fluctuations tend to exhibit larger amplitudes than global means on all time scales (Serreze and Barry 2011). Observed surface air temperature (SAT) records show two Arctic warming periods (1910–1940 and 1970–present) and a cooling period (1940–1970), which might be (partly) attributable to long-term variability of the climate system. It is not clear whether this multidecadal variance in the twentieth century is externally forced by aerosols or internally by mediation of the ocean circulation. Booth et al. (2012) showed that aerosol emissions and periods of volcanic activity explain 76 % of the simulated multidecadal variance in detrended 1860–2005 North Atlantic sea surface temperatures in a state-of-the-art Earth system climate model. The multidecadal variance is, however, also highly correlated with the Atlantic Multidecadal Oscillation (AMO) (Chylek et al. 2009), suggesting that Arctic temperature variability on multidecadal timescales is linked to the Atlantic meridional overturning circulation (AMOC) (Delworth and Mann 2000). In addition, observed

✉ Eveline C. van der Linden
linden@knmi.nl

¹ Royal Netherlands Meteorological Institute, De Bilt, The Netherlands

² Wageningen University, Wageningen, The Netherlands

³ University of Tromsø, Tromsø, Norway

freshwater anomalies in the Nordic Seas are primarily related to salinity changes in Atlantic inflow, suggesting that the AMOC is the driver of multidecadal freshening of the Nordic Seas (Glessmer et al. 2014). Associated with the Arctic SAT variability, the Atlantic water temperature record shows two warm periods, one in the 1930–40s and one in recent decades, and two cold periods, one earlier in the century and one in the 1960–70s, with a time scale of 50–80 year (Polyakov et al. 2004).

Observed Arctic sea ice concentrations also show multidecadal (60–90 year) fluctuations that covary with the AMO and are most pronounced in the Greenland Sea (Miles et al. 2014). Unfortunately, the satellite-based sea ice record is not long enough to track more than one complete cycle. For the 1979–2011 period, observed retreat of Arctic September sea ice extent is about 70 % larger than the reduction simulated by the CMIP5 multi-model mean ensemble (Stroeve et al. 2012). This difference in trends might be, at least partly, attributable to low-frequency natural variability in the climate system. Beitsch et al. (2014) studied a 3000-year unperturbed climate simulation and found 26 Arctic warming episodes caused by natural variability that are comparable with the early twentieth century warming. Also in model simulations it is thus not straightforward to separate anthropogenic trends from natural variability.

In model simulations most mechanisms that potentially influence Arctic climate variability have in common that they are related to changes in meridional heat and fresh water transports between the Arctic and North Atlantic. The heat transports can be related to the ocean, the atmosphere, or both. Given the long memory of the ocean, it is likely that low-frequency variability has its origin there. Using a 1000-year-long segment of a control simulation of the GFDL CM2.1 model, Mahajan et al. (2011) showed that simulated Arctic SAT is significantly correlated with the AMOC, with maximum correlation when the AMOC is leading by 1 year. In addition, Levitus et al. (2009) showed in observations a connection between ocean temperatures at 100–150 m depth of the Barents Sea (BS)—with a multidecadal variability on the order of 4 K—and the AMOC. The AMOC in the EC-Earth climate model has a dominant timescale of 50–60 years (Wouters et al. 2012), with associated positive anomalies of SAT in the BS. Weakening or strengthening of the AMOC can thus weaken or enhance Arctic warming by affecting the ocean heat transport and ocean heat uptake.

Besides ocean transports, atmospheric transports and local feedbacks are found to be related to the SAT variability over the Arctic. In the CCSM2 model the oceanic exchanges between the North Atlantic and Arctic and heat transport into the BS dominate Arctic SAT variability, but there is also a relation between SAT variability and the North Atlantic

oscillation (NAO)/Arctic oscillation (AO) (Goosse and Holland 2005). However, this relation is ambiguous since it is only significantly related to Arctic temperature variability over certain time periods. In the Hadley Centre and Max Planck coupled atmosphere–ocean models, ocean heat transport anomalies affect sea ice cover and surface heat fluxes mainly in the Barents Sea/Kara Sea region to which the atmosphere responds with a modified pressure field (Van der Swaluw et al. 2007; Jungclaus and Koenigk 2010). As a result, variations in atmospheric and oceanic heat transports are strongly coupled and even compensate each other, a phenomenon that was diagnosed as Bjerknes compensation (Bjerknes 1964). Another potential mechanism causing variability in the Arctic is the Arctic Ocean oscillation (AOO), a wind-driven oceanic motion in the Central Arctic that alternates every 5–7 year between cyclonic and anticyclonic circulation regimes (Proshutinsky and Johnson 1997). During the cyclonic regime, the SAT in the Arctic tends to be higher. Even though the relations between SAT variability and atmospheric circulation regimes are less pronounced than those related to ocean heat transport, changes in the ocean heat transport can be weakened or amplified as a result of those atmospheric processes.

Here we will address the multidecadal SAT variability over the Arctic. Since observational records in the Arctic are too short to track multiple multidecadal SAT cycles, we have to use model simulations to study this phenomenon. The focus of our study is the BS region, because it is clear that the BS region plays a key role in the processes that create variability in the entire Arctic system (Smedsrud et al. 2013). We will address the energy budget components in the BS, including their leads and lags as well as their seasonal cycle with respect to SAT. Although it is well-known that sea-ice related feedbacks influence atmosphere–ice–ocean interactions in the Barents and Kara Seas (Årthun and Schrum 2010), these local mechanisms are not yet well-understood on multidecadal timescales. Therefore we will study in detail the local air–ice–ocean interactions that take place over multidecadal cycles.

2 Data and methods

We will focus on the pattern and timescale of low-frequency Arctic SAT variability in coupled models. For this purpose we use the preindustrial simulations of models in the Coupled Model Intercomparison Project phase 5 (CMIP5) (Taylor et al. 2012). Since we are interested in multidecadal variability, the length of the model experiment should be at least 500 years. In this way internal variability due to chaotic variations in the climate system can more accurately be distinguished from semi-oscillatory interannual to decadal variability. This leaves us with a subset of 18 climate

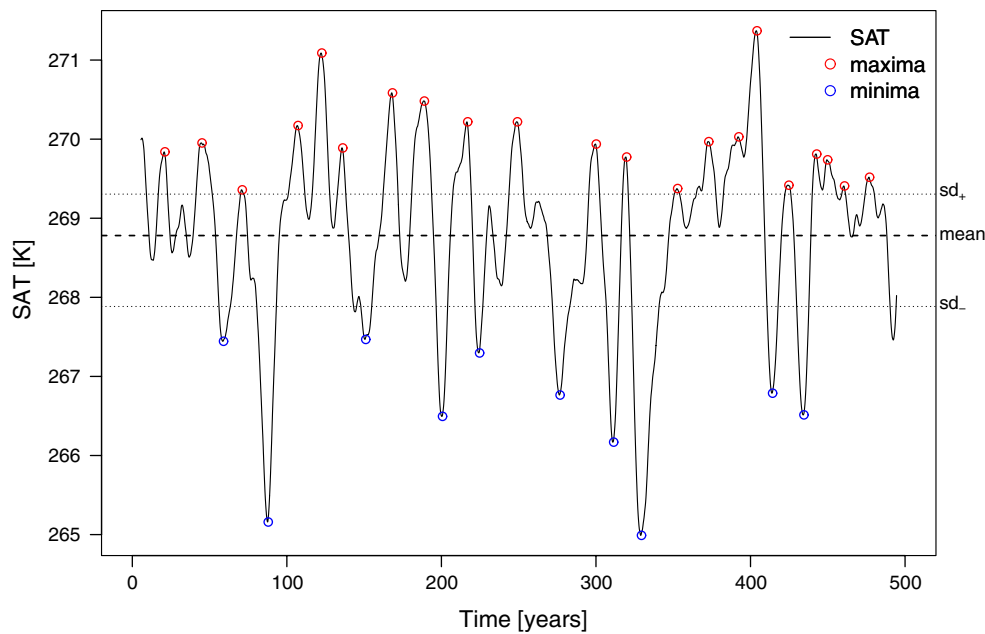


Fig. 1 Smoothed time series of surface air temperature over the Barents Sea. The red and blue dots represent the selected 11-year running local maxima and minima for the computation of the composites. We used two different standard deviations: sd_+ (sd_-) is defined as the

standard deviation of the warm (cold) phase. Only the values that are larger (smaller) than one positive (negative) standard deviation sd_+ (sd_-) from the mean are considered as maxima (minima)

models. Following Massonnet et al. (2012), we only select models that reasonably simulate the sea ice extent, including its seasonal cycle and trend over 1979–2010, and sea ice volume, which leaves only 5 models. For brevity, we will present results of only one of these models in detail, namely ACCESS1.3. Its smoothed time series of SAT over the BS is shown in Fig. 1. This model exhibits a reasonable and stable representation of key diagnostics of ocean climate performance in the preindustrial control simulations, including the meridional overturning circulation and poleward heat transport maximum (Marsland et al. 2013).

From observations we know that the dominant time-scales of multidecadal variability in ocean temperatures in the North Atlantic have two main periods: the long (50–70 years) and the shorter period (20–30 years) (Frankcombe and Dijkstra 2010). BS surface atmospheric temperatures in ACCESS1.3 show a 99 % significant peak at 26 years and a 95 % significant peak at 62 years (Fig. 2), indicating that the time scales of its variability are close to observations. We compared the simulated pattern of annual mean Arctic decadal temperature variability (Fig. 3) with the early twentieth century warming (Bengtsson et al. 2004), which is thought to be dominated by internal climate variability. This comparison shows that both the observed and simulated variability exhibit a dominant signal over the BS. The results presented here are likely representative for a broaden suite of CMIP5 models, since most models have qualitatively similar characteristics of simulated variability.

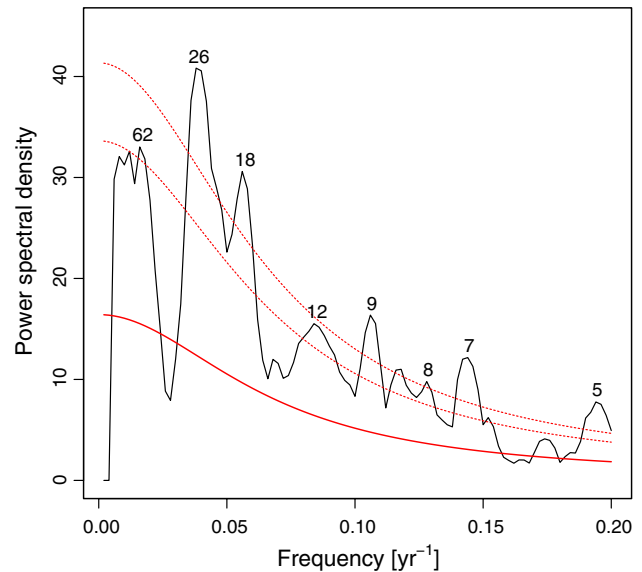


Fig. 2 Spectrum of the annual mean surface air temperature over the Barents Sea (model ACCESS1.3). The two dashed red lines represent the 95 and 99 % significance levels of the theoretical red noise spectrum (red line) with the autocorrelation and standard deviation of the time series. The numbers above the significant local maxima represent the periods that are associated with the local maxima in years

In our study, the BS is defined as the area between 20–70°E and 70–80°N. All variables that will be shown and discussed have been detrended and deseasoned. To

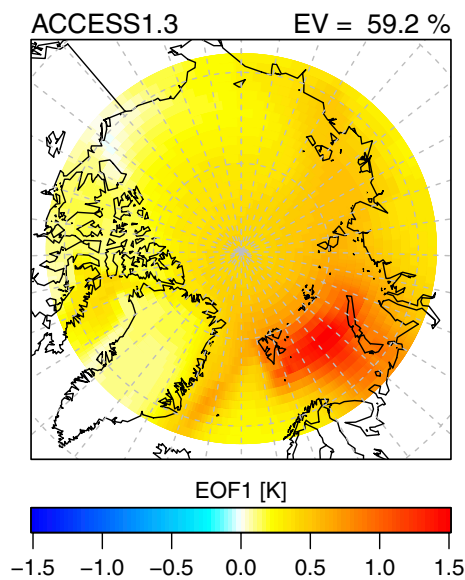


Fig. 3 First empirical orthogonal function (EOF1) of the surface air temperature over the Arctic in ACCESS1.3. The EOF represents the amplitude relative to one standard deviation of the associated principal component. EV is the percent variance explained by EOF1

emphasize decadal time scales the time series are smoothed with an 11-year running Welch window, which was normalized to have an average power of unity.

3 Barents Sea variability characteristics

In this section we explore the low-frequency variability of SAT in the Arctic. The first empirical orthogonal function (EOF1) of Arctic SAT shows that annual mean Arctic SAT variability is dominated by variability over the BS region (Fig. 3). In ACCESS1.3, EOF1 explains 59 % of the total variability in the Arctic. The temporal behaviour of the corresponding principal component of SAT in the Arctic is closely linked to the BS-averaged SAT, with a correlation of 0.90. Both the time series of the first principal component and the time series of BS-averaged SAT exhibit a red spectrum, with enhanced power at low frequencies. The smoothed time series and spectrum of the annual mean SAT anomalies over the BS are presented in Figs. 1 and 2, respectively. The principal component and SAT index time series both have a dominant periodicity of about 26 years. The smoothed SAT anomalies over the BS range from -3.8 to 2.6 K, with a standard deviation of 1.1 K. Periods with a positive SAT anomaly are defined as a warm phase, and periods with a negative SAT anomaly as a cold phase. The BS is in a warm phase for 60 % of the time. This skewed behavior indicates that nonlinear processes likely play a role in the SAT variability. Despite this skewed behavior we will see later on that the feedbacks in the warm and cold phases are qualitatively similar, but opposite in sign.

4 Energy budget analysis of the Barents Sea

To investigate what mechanisms are important during the multidecadal cycles of SAT variability, we analyze the flows of energy to and from the BS. The energy budget for the atmosphere in an enclosed region in the Arctic (Fig. 4) can be written as

$$dE_A/dt = F_{TOA} - F_{SFC} - \nabla \cdot AHT \approx 0, \quad (1)$$

where we assume that the atmosphere has zero heat storage ($dE_A/dt \approx 0$). The net downward top-of-atmosphere radiation flux (F_{TOA}) is obtained from differencing net absorbed shortwave radiation and outgoing longwave radiation. The total downward surface flux (F_{SFC}) is computed as the sum of the net radiative flux (the net longwave and shortwave radiative fluxes), and the turbulent heat fluxes (sensible and latent). The convergence of atmospheric heat transport ($-\nabla \cdot AHT$) into the BS is approximated as the residual of F_{SFC} and F_{TOA} . The ocean energy budget in an enclosed basin in the Arctic equals

$$dE/dt = F_{SFC} - \nabla \cdot OHT. \quad (2)$$

The convergence of ocean heat transport ($-\nabla \cdot OHT$) into the basin is approximated as the residual of F_{SFC} and ocean heat storage (dE/dt). The ocean heat content (E) is calculated as the volume integral of $\rho_0 c_p \theta$ over the basin, where ρ_0 is the reference density for the Boussinesq approximation, c_p is the specific heat capacity for seawater, and θ is the potential temperature. OHT and dE/dt are divided by the surface area of the basin in order to compare them to the units of the other fluxes ($W m^{-2}$).

To assess the realism of the simulated energy budget, the modelled Arctic energy budget (the region north of $70^\circ N$) is compared with the energy budget using present-day observations (Serreze et al. 2007). The simulated total heat transport into the Arctic is slightly larger than in the observations, but the ratio of OHT to AHT is similar. Given that the heat budget is not closed in the real-world data, and that we use preindustrial climate conditions instead of present-day conditions, ACCESS1.3 seems to simulate the Arctic heat budget sufficiently realistic.

In the mean preindustrial climate state, both OHT and AHT are directed towards the BS mainly due to the equator-to-pole temperature gradient (Fig. 4). The mean F_{SFC} is directed upward, i.e. the ocean loses heat to the atmosphere. The net radiation at the top-of-atmosphere (F_{TOA}) is outgoing. On average the atmosphere contributes 59 % to the total energy transport into the BS region, and the ocean 41 %. Almost all the heat that enters the BS through OHT is used to either melt sea ice or heat the atmosphere through surface fluxes. The dE/dt is very small, showing that the simulated preindustrial climate is close to

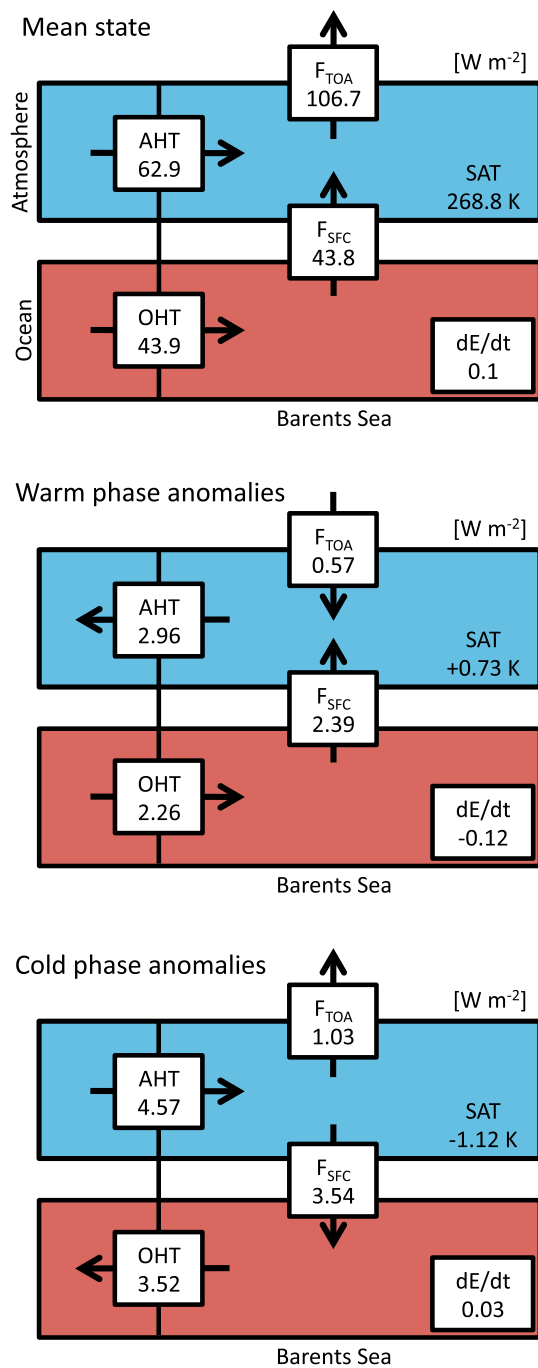


Fig. 4 Energy budget components in the preindustrial climate of the Barents Sea in $W m^{-2}$. The *top figure* shows the energy flows in the mean climate state, and the *middle* and *bottom figure* the average anomalies in the warm and cold phase, respectively. The *arrows* point in the direction of the anomalies

equilibrium. All energy budget components exhibit a low-frequency variability with a timescale of 26 years. The mean energy budget anomalies of the BS averaged over the warm and cold phases are also shown in Fig. 4. During warm phases, OHT, F_{SFC} and F_{TOA} enhance surface

warming, whereas AHT dampens it. During cold phases, all anomalies are of opposite sign, and also slightly larger in magnitude than in the warm phases. This is related to the skewed behavior of the SAT time series, and for this reason warm phases last longer than cold phases. The magnitude of dE/dt is small in both warm and cold phases, indicating that ocean heat storage is not in phase with fluctuations in SAT, but the ocean heat content itself is (i.e. little change at the peaks). Large amplitude variations of AHT and OHT are of opposite sign on multidecadal timescales, a characteristic that might be related to Bjerknes compensation. An explanation for this is that the atmospheric response to increased (decreased) surface fluxes is a decreased (increased) meridional temperature gradient, leading to a decreased (increased) heat transport by baroclinic eddies, and thus a weaker poleward transient atmospheric energy transport (Shaffrey and Sutton 2006; Van der Swaluw et al. 2007). However, since we have no information on the direction of the atmospheric transport, we can only conclude that AHT is directed out of the BS when there is a gain of heat by ocean heat transport.

4.1 Leads and lags

To obtain a better understanding of the mechanisms behind BS variability on the multidecadal timescale we explore the lead-lag relationships between BS-averaged SAT and the energy budget components in the BS. To obtain more information about the causes and effects of the energy flow, we compute cross-correlations between the energy budget variables and SAT over the BS. In accord with Bjerknes compensation, the smoothed OHT and AHT are strongly anticorrelated, with maximum anticorrelation (-0.97) when OHT is leading AHT by 17 months (Fig. 5). The absolute correlation between OHT and SAT is maximum for OHT into the BS leading SAT by 15 months (not shown). AHT leaving the BS lags SAT by 6 months. From this it is clear that the atmosphere responds to SAT changes by compensating for the increased ocean heat transport. However, F_{SFC} that can act to warm the atmosphere lags SAT by 7 months over the BS as a whole. In Sect. 6 we will show that the spatial pattern of the F_{SFC} anomalies over the BS reveals that it can be subdivided into an eastern and western part. The western part, where the sign of the response is negative, is leading changes in SAT, and the central/eastern part is lagging changes in SAT. This east-west difference in response time is likely linked to sea ice coverage.

In the cross correlation method the computed leads and lags take into account the entire period. To investigate the leads and lags that are active around the peak periods only we define two composites: a warm one and a cold one. The warm (cold) composite consists of the local SAT maxima (minima) of the smoothed time series

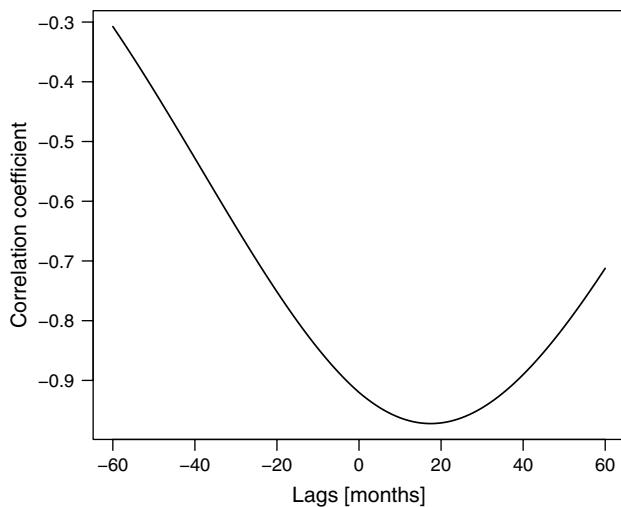


Fig. 5 The correlation of the ocean heat transport with the atmospheric heat transport into the BS. At positive lags OHT is leading

that deviate more than one standard deviation from the mean (Fig. 1), in which 24 months before and after each peak are included in the composite. These SAT time indices for the warm and cold composites are used to make composites of other variables over the same time periods. Figure 6 shows the mean warm and cold composites of all energy budget components averaged over the BS. Before the mean was computed, all local SAT extremes were aligned on top of each other. The location of the energy budget component peaks relative to the SAT maxima provides a measure of their leads/lags. It seems clear, in this model, that the ocean drives the changes in the BS, and that the atmosphere is mostly responding to the ocean. We do not know, however, if the ocean drives the variability or that it only plays a mediating role. The question rises whether the OHT variability is due to variations in the strength of the ocean circulation (volume transport) or due to variations in the temperature stratification (inflow and outflow temperatures) of the ocean. To assess the variability of the strength of the circulation we study the time series of the AMOC index (Fig. 7). The correlation between OHT into the BS and the AMOC index is 0.40, implying that about 16 % of the low-frequency variability in OHT can be attributed to the AMOC strength. This value is similar to the value found by Mahajan et al. (2011). Note that at 60°N, however, OHT is dominated by heat transport due to the sub-polar gyre (Beitsch et al. 2014). The gyre circulation might play an important role in the total heat transport into the Barents Sea in comparison with the AMOC-driven heat transports. The remaining variability can thus be explained by heat transport variations due to the sub-polar gyre and variations in temperature stratification.

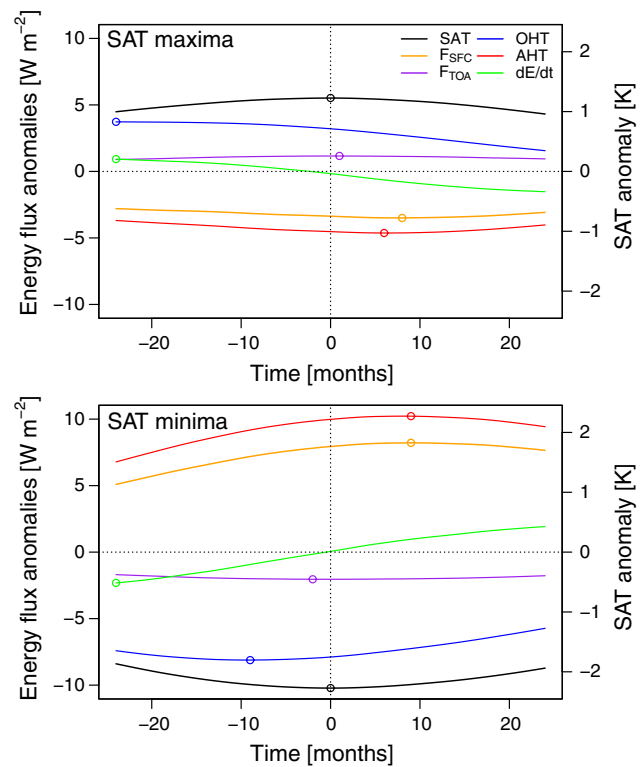


Fig. 6 Energy budget components of the Barents Sea in the warm (*top*) and cold (*bottom*) composites of the Barents Sea. The *open circles* represent the absolute maxima within each composite. Their relative position to the SAT maxima/minima gives an indication of their leads/lags

5 Seasonal cycle in variability

The multiyear variability in the BS-averaged SAT is not equally spread throughout the year (Fig. 8). Winter months exhibit four times larger multidecadal variability compared to the summer months. Synoptic eddy activity is strongest in winter and hence AHT exhibits most variations in winter. On the other hand, F_{TOA} varies more in summer when there is a larger influx of solar radiation. OHT and dE/dt show two periods of enhanced variability in summer and winter. SST exhibits more decadal variability at the end of summer when SIC is low, and sea ice is not restricting the SST to melting point temperature. SIC variability is also lower at the end of summer, just because there is less sea ice to vary. When we look more closely at the variability of the surface energy balance fluxes (not shown), we infer that all components exhibit most variability in winter, except the SW fluxes. The SW fluxes are most variable in May–June, due to a combination of high SIC in late spring and high solar insolation in June.

Monthly EOFs of Arctic SAT show that the variability pattern has dominant variability over the BS, which is most pronounced in December–April and July–August (Fig. 9). In winter, the amplitude of the variability is much larger

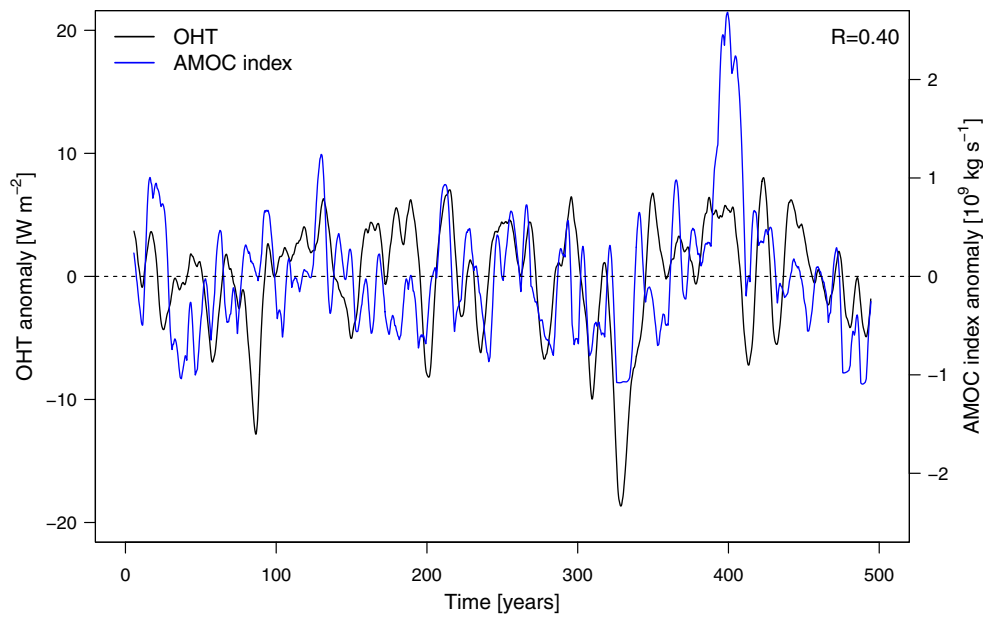


Fig. 7 Smoothed time series of OHT into the BS and the AMOC index. Here we define the AMOC index as the maximum value of the meridional overturning mass stream function between 500 and 2000 m depth, and between 15 and 65°N

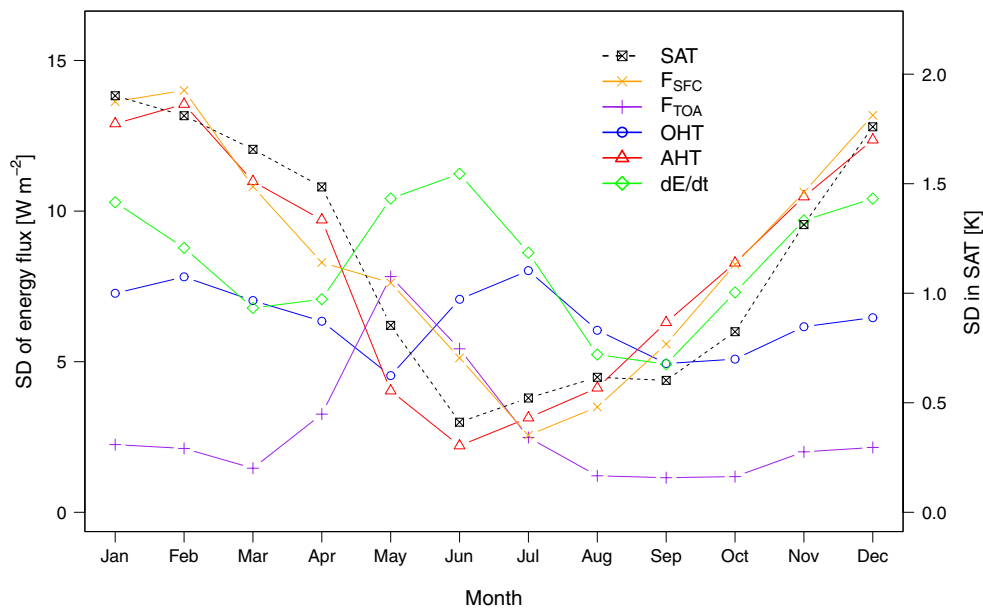


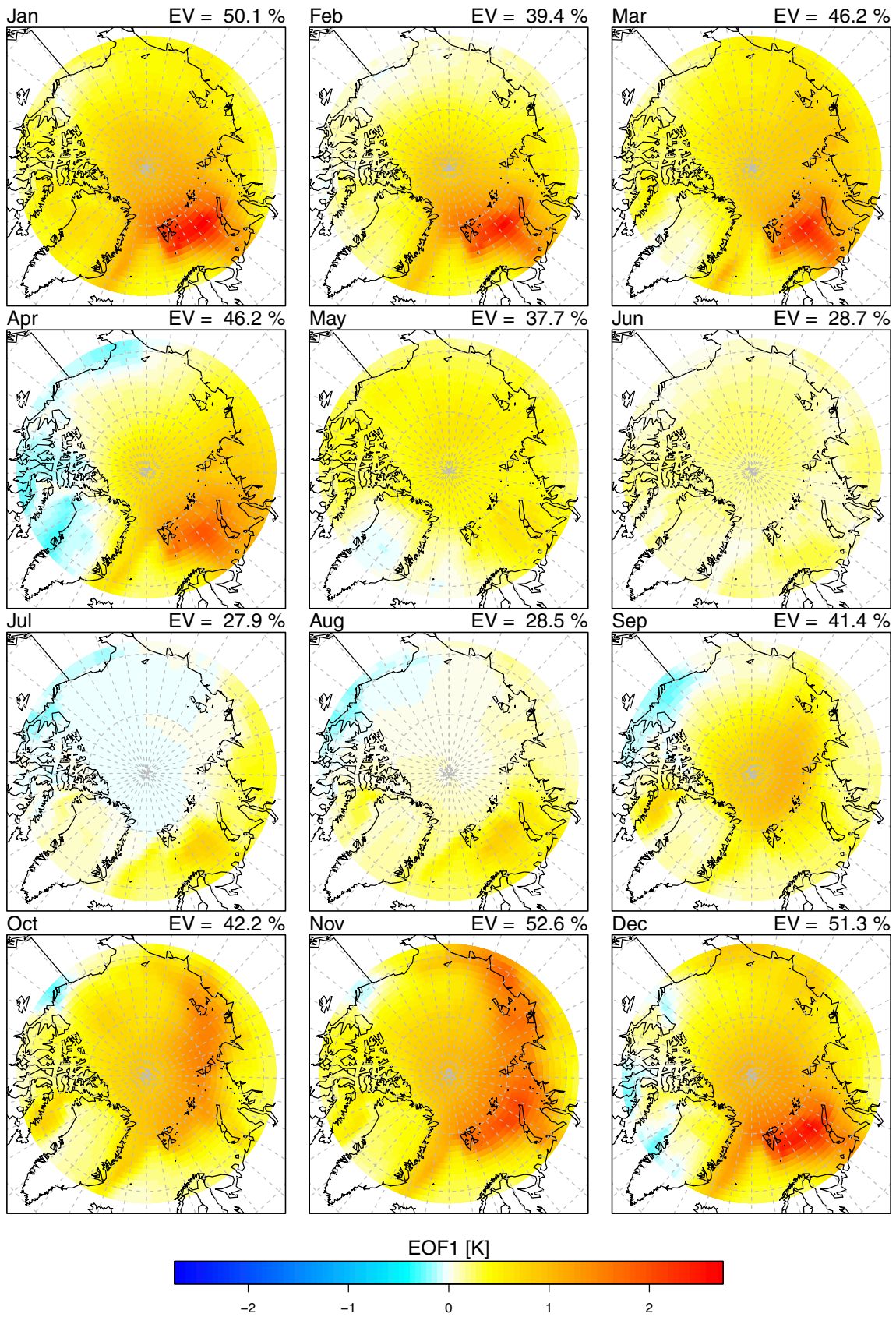
Fig. 8 Multiyear monthly standard deviation for the Barents Sea energy budget components and SAT

than in summer. Therefore for summer months, the pattern is not clearly visible, since the EOFs are plotted on the same scale. In spring and autumn the dominant mode of temperature variability is more spatially uniform. The summer/winter versus spring/autumn division in the pattern of SAT variability is in agreement with variability in OHT, which likely drives variability in the BS region as shown before. In May-June and September-November dominant variability is less restricted to the BS. On multidecadal

timescales the driver of the dominant variability is thus present throughout the year, but it is most enhanced during the winter months.

6 Local characteristics

In this section we investigate what variables covary with the regional average SAT over the BS to determine how



◀ **Fig. 9** Monthly EOF1 of smoothed surface air temperature over the Arctic. The EOF analysis is applied after smoothing the time series for each month. The EOFs represent the amplitude relative to one standard deviation of the associated principal components. EV is the percent variance explained by EOF1

the OHT influences SAT. For this purpose, linear regressions were computed between the time series of several local variables at each grid point in the Arctic versus the time series of the BS-averaged SAT (Fig. 10). Clearly, the

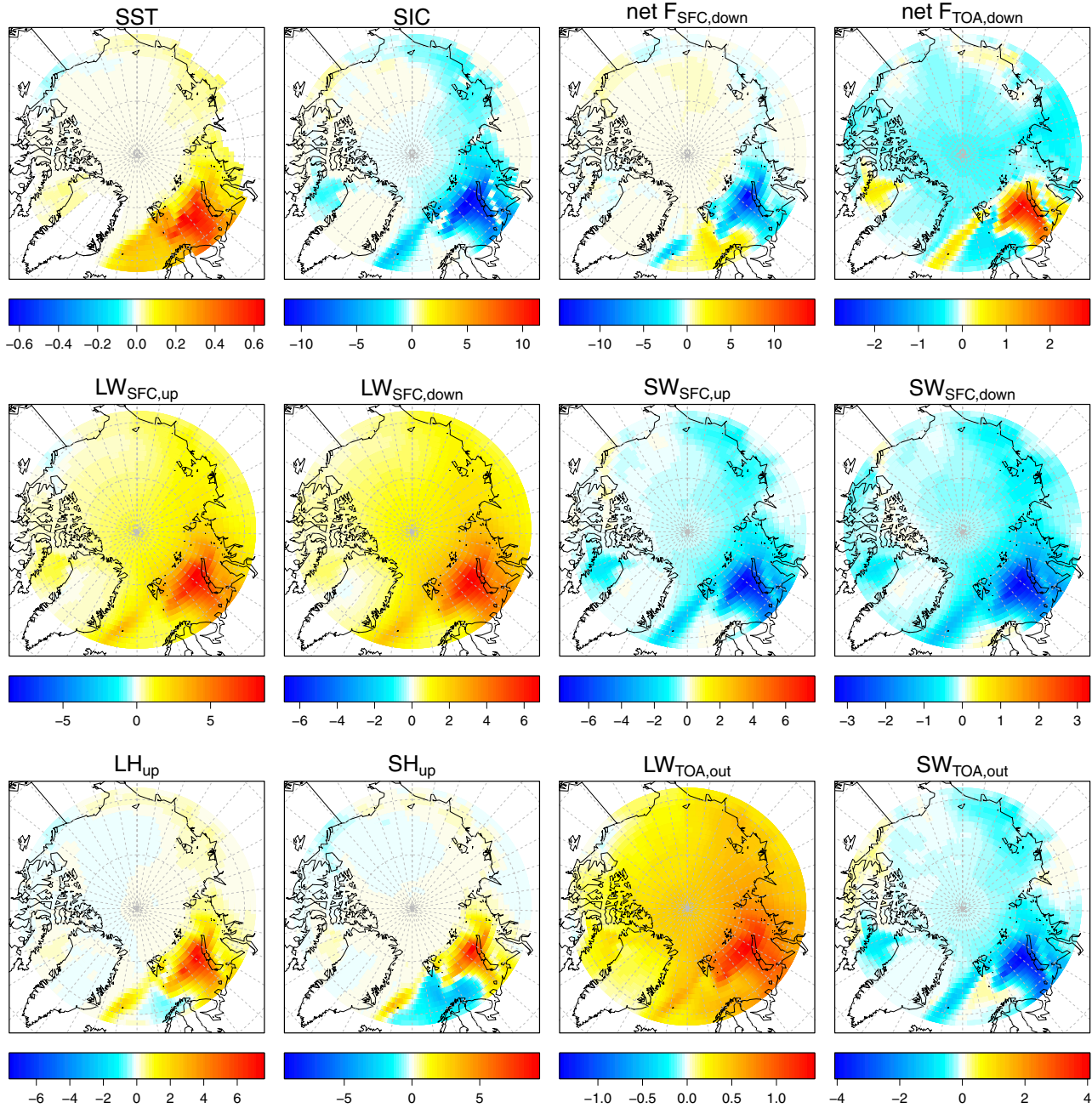


Fig. 10 Regression coefficient maps of surface and TOA variables on Barents Sea-averaged SAT. The *subscripts behind the variable names* refer to the sign of the reference state. Units are in $K K^{-1}$ for SST, $\% K^{-1}$ for SIC and $W m^{-2} K^{-1}$ for the heat fluxes

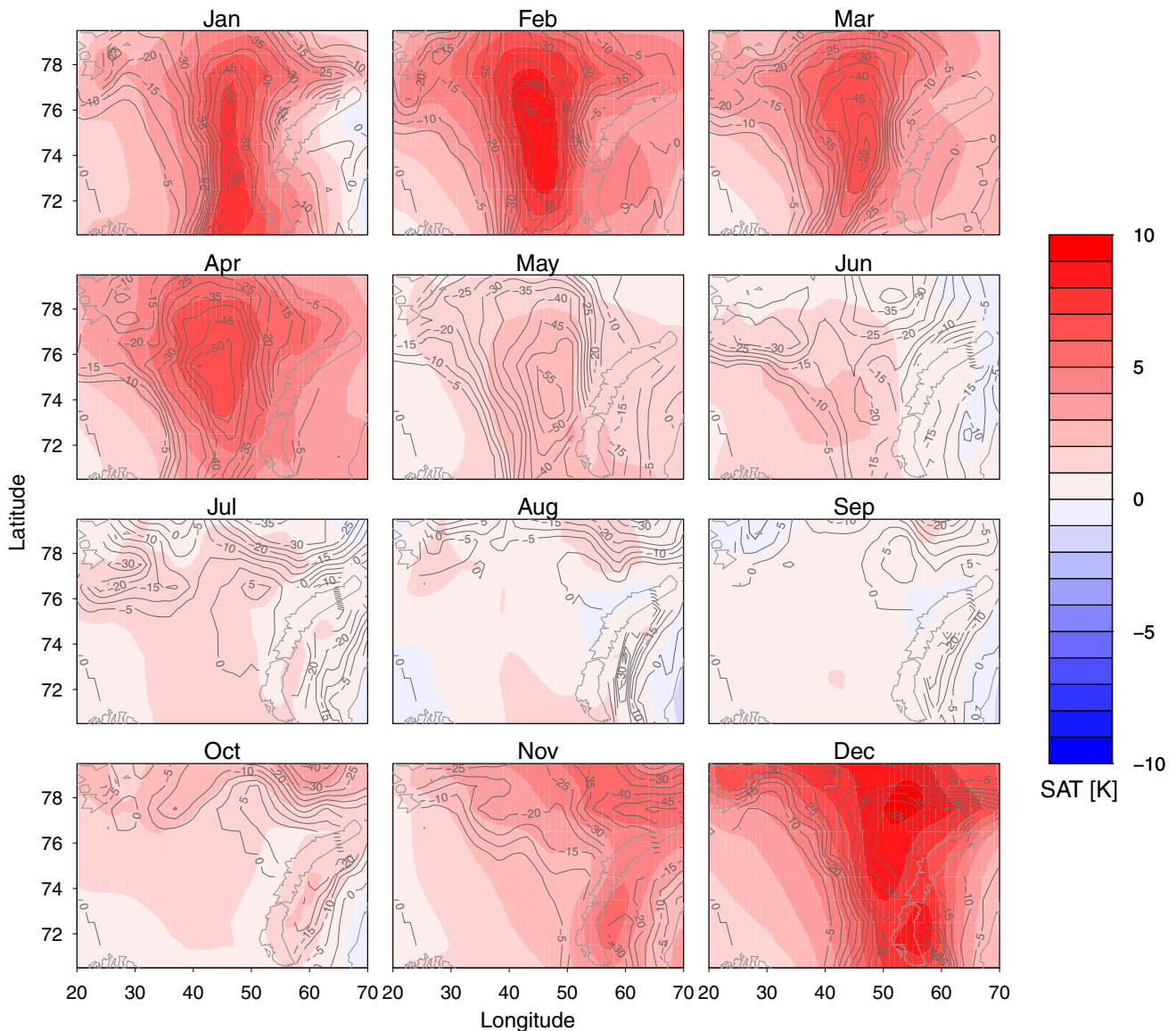


Fig. 11 Monthly composite differences of SAT (*colorscale*) and SIC (*isolines*, in %) as function of latitude and longitude over the Barents Sea. The cold composites are subtracted from the warm composites

Arctic response of all surface variables is strongest in the BS region. We use the difference between the mean of the cold and warm composites as a measure of the amplitude of the low-frequency variability. For SAT the largest differences between the composites are found over the central BS in December, with peaks up to +9 K (Fig. 11). From January until April, SAT peaks are found slightly more to the west. From May until October, the SAT differences are smaller than 4 K over the whole BS. Since ice melts during warm periods, sea ice cover is reduced during the warm phase, and extended during the cold phase. The co-variability of sea ice concentration with BS-averaged SAT acts mainly local over the BS. In a warm phase,

OHT is transporting energy to the BS, melting the sea ice at most locations and increasing SAT over the BS. The largest composite differences in sea ice concentration are found in the winter and spring months in the central BS, owing to retreat of the ice edge. When sea ice retreats, a clear atmospheric response is indicated by anomalous low pressure over the Greenland and Barents Seas (not shown). The differences between the warm and cold composites in SST are largest in the summer months, with maximum differences in June (+2 K). Since the BS clearly dominates Arctic variability, the monthly surface energy balance components in the BS will be discussed in detail in the next subsection.

6.1 Surface energy balance

The variability in sea ice has huge consequences for F_{SFC} . BS-averaged F_{SFC} is upwards (i.e. ocean to atmosphere) in the mean climate, and is enhanced during warm phases and reduced during cold phases (Fig. 10). The surface response, however, varies spatially owing to the sea ice variability in the central/eastern BS. During a warm phase, net F_{SFC} is reduced in the western BS and over the central Arctic, whereas over the central/eastern BS the heat fluxes are enhanced. The amplitude of variability in surface heat fluxes is largest in winter (Fig. 8). In December the F_{SFC} composite differences are largest in the western BS, where the surface fluxes are reduced by up to 84 W m^{-2} in the

warm composite relative to the cold composite (Fig. 12). In January and February the surface heat flux differences are largest in the central BS, where in the warm composite they are enhanced by up to 146 W m^{-2} . This shift in month and region is likely related to the eastward shift of the sea ice edge, and may be very model dependent, since the sea ice edge varies between models.

6.1.1 Longwave radiation

The net flux of longwave radiation in the mean climate is directed from ocean to atmosphere. $LW\uparrow$ and $LW\downarrow$ fluxes are both enhanced when SAT is higher (Fig. 10), as there is a direct relation between LW radiation and temperature.

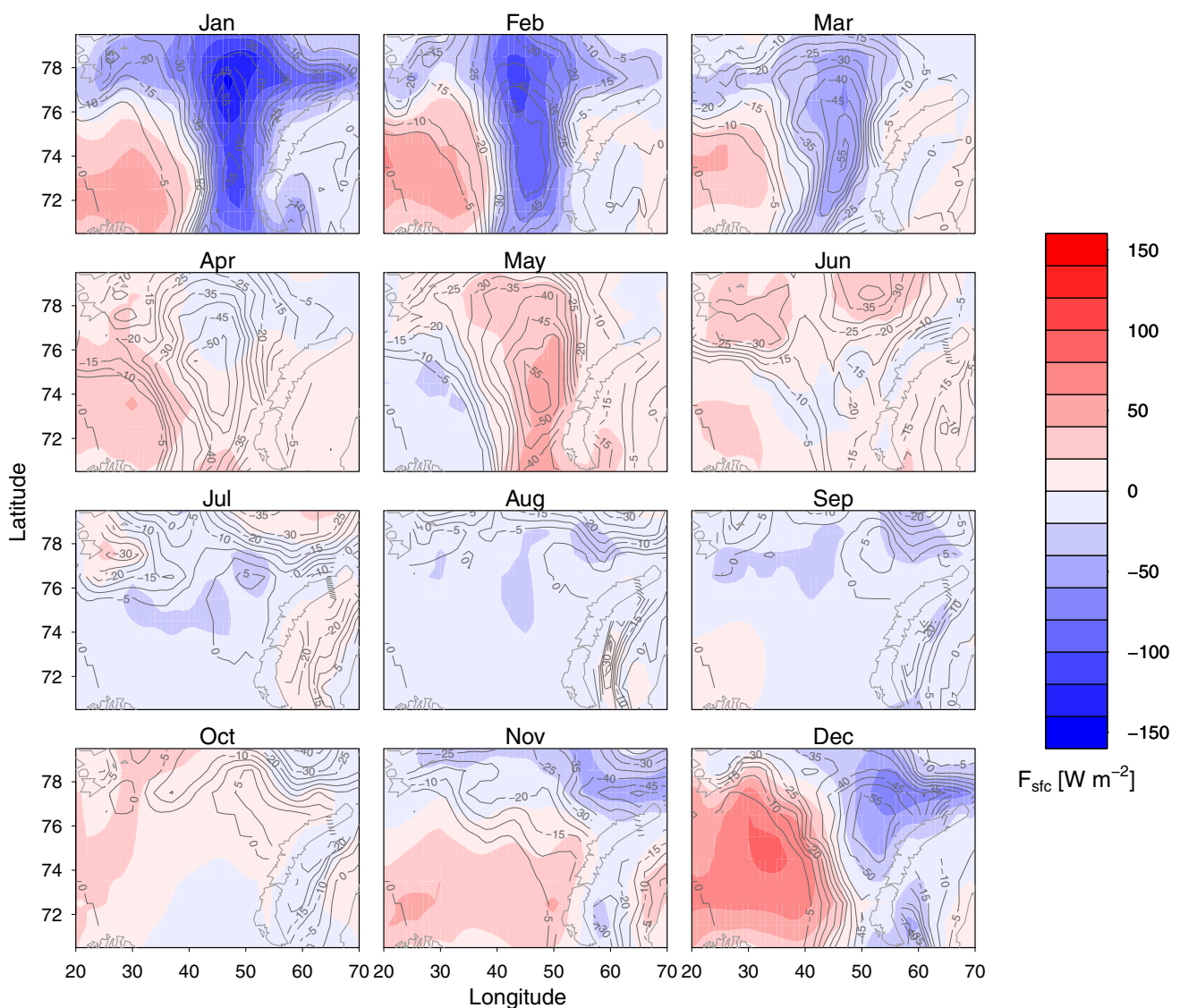


Fig. 12 Monthly composite differences (warm–cold) of net F_{SFC} (colorscale) and SIC (isolines, in %) over the Barents Sea. F_{SFC} is defined positive downward, which means that positive values (red)

indicate a reduced upward heat flux and negative values (blue) indicate an enhanced upward heat flux

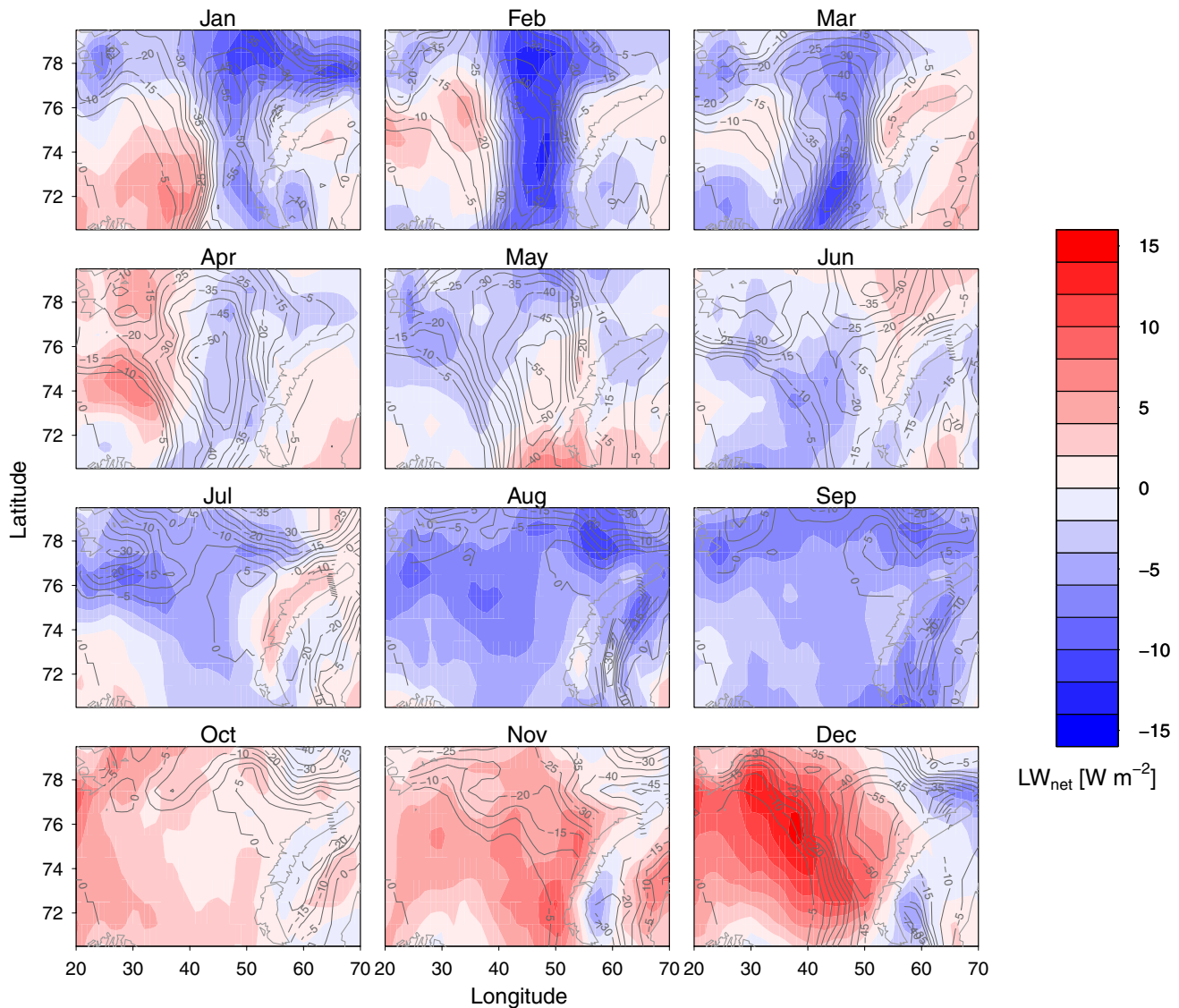


Fig. 13 Monthly composite differences (warm–cold) of LW net radiation ($LW_{\downarrow}-LW_{\uparrow}$; colorscale) and SIC (isolines, in %) over the Barents Sea. Positive values (red) indicate a reduced upward flux and negative values (blue) indicate an enhanced upward flux

LW_{\uparrow} is governed by the surface temperature and thus sea ice, whereas LW_{\downarrow} is dictated by the temperature, humidity and cloudiness of the atmosphere aloft. Maximum LW_{\downarrow} variability is found over the central BS during the winter months (with composite differences up to $48 W m^{-2}$ in December). LW_{\uparrow} variability is maximum in the central BS in the winter months as well, but is concentrated later in the winter season in January/February (up to $48 W m^{-2}$). As a result, during warm phases the net longwave radiation flux is reduced over most of the BS in December, while in February the longwave radiation flux is enhanced over most of the BS (Fig. 13). In January, a dipole pattern is visible where net longwave radiation is reduced over the western BS, but enhanced over the eastern BS.

6.1.2 Shortwave radiation

Both SW_{\uparrow} and SW_{\downarrow} are reduced during warm phases (Fig. 10). Since there is less sea ice, less SW radiation is reflected upward. The effect is clearly dominant in May, when the SW_{\uparrow} in the central BS is reduced by up to about $115 W m^{-2}$ in the warm composite relative to the cold composite. At this time of the year sea ice concentration has decreased by up to 59 % in the central BS and incoming solar radiation is close to its maximum. During warm phases, SW_{\downarrow} is also smaller by up to about $45 W m^{-2}$ for the composite difference in May. This is likely caused by an increase in cloudiness in relation to reduced sea ice and enhanced surface evaporation. In addition, the

back-scattering by the atmosphere (multiple reflection) also affects SW_{\downarrow} . The increased absorption of SW radiation over transition regions from sea ice to open water is dominant over the cloud and back-scattering effects, enhancing the net shortwave flux from the atmosphere to the ocean (Fig. 14).

6.1.3 Latent and sensible heat fluxes

The latent and sensible heat fluxes are directed upward in the mean climate, warming the atmosphere, especially in the western BS in winter. In the major part of the BS the upward turbulent fluxes are enhanced during the warm phases (Fig. 15), dampening ocean heating but warming

the atmosphere. The increase in upward LH will likely enhance the cloudiness by adding more water vapour to the atmosphere, which in turn influences LW_{\downarrow} and SW_{\downarrow} radiation. The increases in turbulent fluxes are dominant in January and February and in the central BS. However, the western part of the BS and adjacent section of the Norwegian Sea exhibit turbulent fluxes that are reduced during warm phases, especially SH. This negative relation is dominant in December. A feature that can explain the differences between the west and central BS, is the presence of (seasonal) sea ice cover in the BS, compared to no sea ice in the Norwegian Sea. Sea ice insulates the ocean from the atmosphere. When sea ice is present (cold periods) the ocean-atmosphere heat fluxes are strongly reduced,

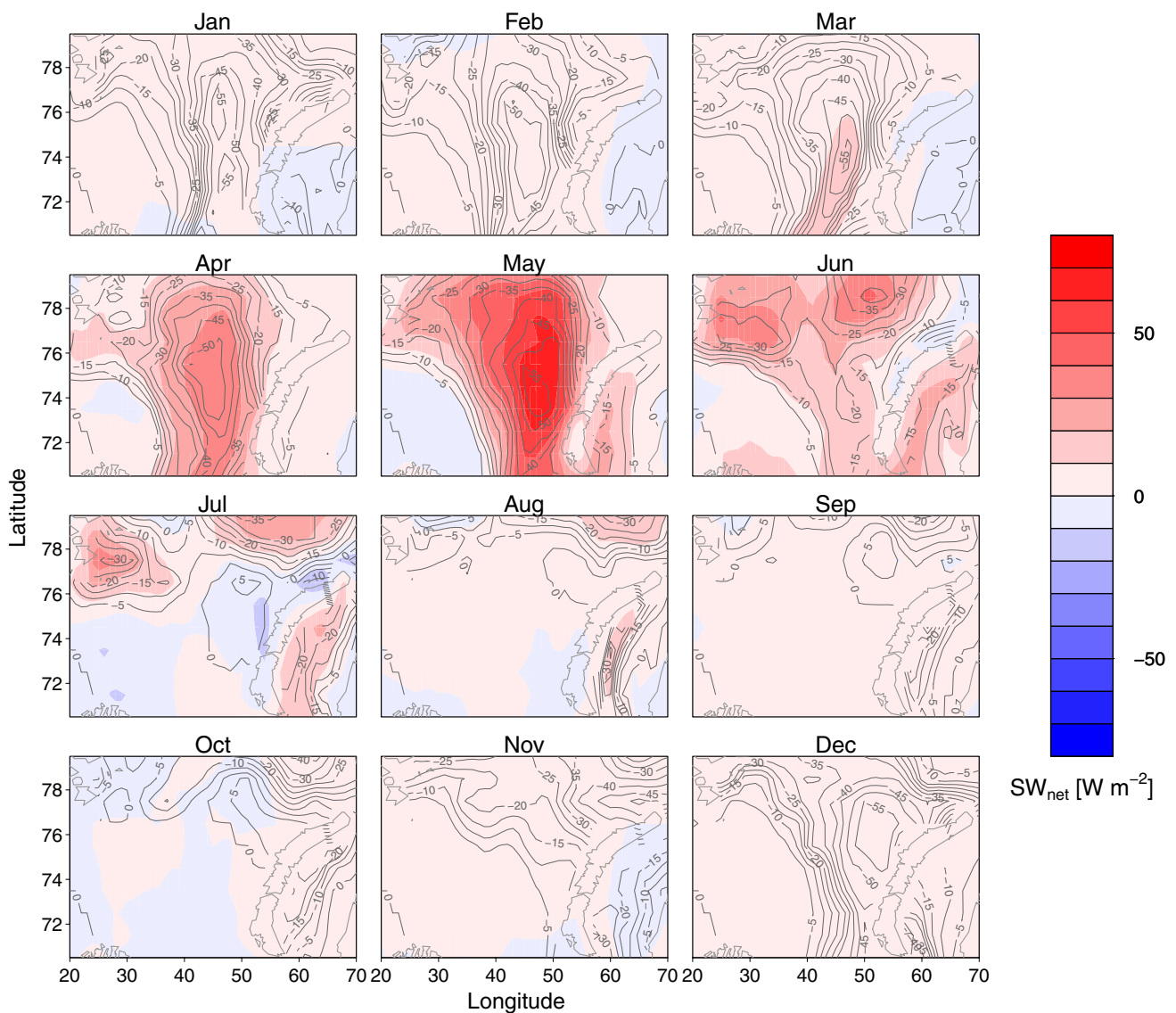


Fig. 14 Monthly composite differences (warm-cold) of SW net radiation ($SW_{\downarrow}-SW_{\uparrow}$; colorscale) and SIC (isolines, in %) over the Barents Sea. Positive values (red) indicate an enhanced downward flux and negative values (blue) indicate a reduced upward flux

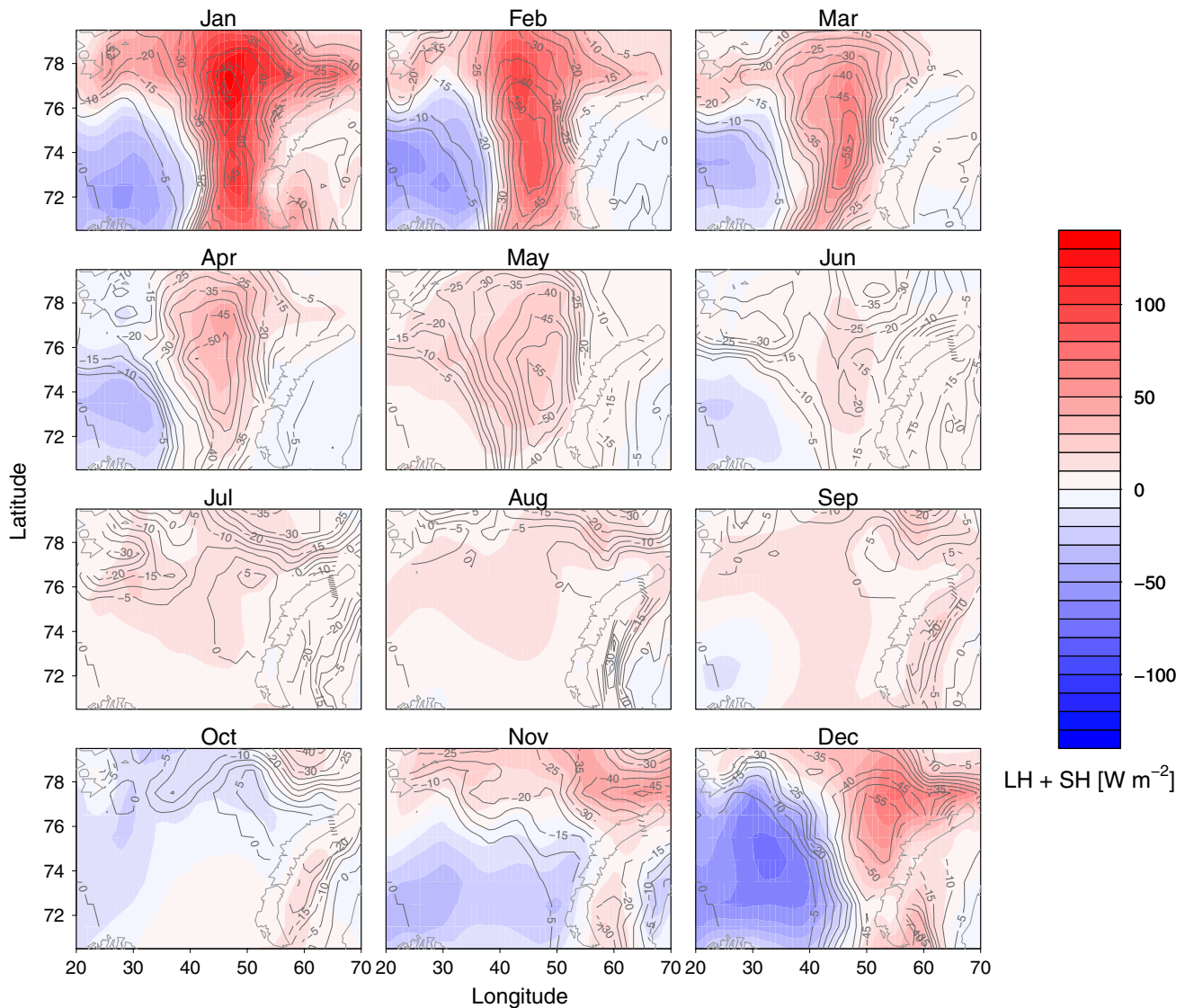


Fig. 15 Monthly composite differences (warm–cold) of the net turbulent flux (LH + SH; colorscale) and SIC (isolines, in %) over the Barents Sea. Positive values (red) indicate an enhanced upward flux and negative values (blue) indicate a reduced upward flux

whereas in warm periods, when the ice cover is absent, ocean–atmosphere fluxes are enhanced. On the other hand, to the west of the BS, sea ice cover is absent in both warm and cold periods. In cold periods, the cold atmosphere over the open ocean takes up heat from the ocean, especially in winter, so that the heat flux is directed from ocean to atmosphere.

To summarize, the net surface energy fluxes over the central/eastern BS from the ocean towards the atmosphere are enhanced during warm phases, pointing towards the ocean as the driver of the BS SAT variability. During warm phases the advected heat input by the ocean is augmented by short-wave radiation and reduced through longwave radiation and latent and sensible heat loss. Sea ice plays a key role in this mechanism (Van der Swaluw et al. 2007). Sea ice separates

the atmosphere from the ocean, creating large temperature gradients between them. When during a warm phase sea ice coverage changes to open water, surface fluxes are enhanced compared to regions that are permanently open water or sea ice-covered in both warm and cold phases. This transition region is located in the central/eastern BS, where the ice edge is located in the preindustrial climate.

7 Summary and conclusions

The role of different energy budget components in low-frequency Arctic climate variability are examined in a 500-years simulation under preindustrial conditions of the ACCESS1.3 model. The multidecadal surface air

temperature (SAT) variability in this model is qualitatively representative for other coupled climate models in terms of the spatial pattern of dominant variability. The dominant mode of Arctic variability in SAT features multidecadal fluctuations centered over the BS region. Locally in the BS, peak-to-peak differences in low-frequency SAT fluctuations are as large as 9 K. This variability exhibits a periodicity with a dominant time scale of 26 years, which is similar compared to most other fully coupled climate models. The ocean heat transport leads SAT variability by more than 1 year, indicating that it drives Arctic SAT variability. Atmospheric heat transport is of opposite sign, and acts to counteract oceanic warming over the BS. It thus compensates the warming that is due to ocean heat transport, a feature that is likely related to Bjerknes compensation (Bjerknes 1964). The spatial pattern of dominant Arctic SAT variability over the BS is present in winter and summer, but not in spring and autumn. The months with a dominant BS variability pattern coincide with the season of maximum variability of OHT into the BS, further confirming that the ocean is indeed driving Arctic SAT variability. Our analysis of the ACCESS1.3 results are in agreement with earlier findings that ocean heat transport plays a dominant role in Arctic climate variability (Mahajan et al. 2011; Goosse and Holland 2005). In turn, changes in OHT might be influenced by the Atlantic meridional overturning circulation (AMOC), which is found to be significantly related to OHT and explains 16 % of the low-frequency variability. The remaining variability can be explained by heat transport variations due to the sub-polar gyre and variations in temperature stratification.

More information about local processes is obtained by studying warm and cold composites of the multidecadal cycles by month. We find that although ocean heat transport into the BS triggers the variability Arctic-wide, it is mostly amplified locally at the location of the sea ice edge in the BS. In areas where there is a transition from sea ice to open water during warm phases, the surface fluxes are enhanced in January and February. In areas with no sea ice in both warm and cold phases, the surface fluxes are reduced mainly in December. As a result, the surface fluxes are enhanced in the late winter season, and reduced during the early winter in warm phases compared to cold phases. This implies that sea ice growth takes place later in the year, and at higher latitudes in the warm phase. The location where the transition of sea ice to open water takes place determines the location of most variability in surface fluxes, and thus variability in SAT. Sea ice thus plays a key role in the transmission of heat from the ocean towards the atmosphere on multidecadal timescales, as was also suggested by Van der Swaluw et al. (2007).

The multidecadal variability in SAT has to be considered in assessments of Arctic warming and cooling trends,

which can be enhanced or reduced by this type of variability. This also implies that differences between simulated and observed warming might be partly attributable to natural low-frequency variability.

References

- Årthun M, Schrum C (2010) Ocean surface heat flux variability in the Barents Sea. *J Mar Syst* 83(1):88–98
- Beitsch A, Jungclaus JH, Zanchettin D (2014) Patterns of decadal-scale Arctic warming events in simulated climate. *Clim Dyn* 43(7–8):1773–1789
- Bengtsson L, Semenov VA, Johannessen OM (2004) The early twentieth-century warming in the Arctic—a possible mechanism. *J Clim* 17(20):4045–4057
- Bjerknes J (1964) Atlantic air–sea interaction. *Adv Geophys* 10(1):82
- Booth BB, Dunstone NJ, Halloran PR, Andrews T, Bellouin N (2012) Aerosols implicated as a prime driver of twentieth-century North Atlantic climate variability. *Nature* 484(7393):228–232
- Chylek P, Folland CK, Lesins G, Dubey MK, Wang M (2009) Arctic air temperature change amplification and the Atlantic Multidecadal Oscillation. *Geophys Res Lett* 36(14):L14801
- Delworth TL, Mann ME (2000) Observed and simulated multidecadal variability in the Northern Hemisphere. *Clim Dyn* 16(9):661–676
- Frankcombe LM, Dijkstra HA (2010) Internal modes of multidecadal variability in the Arctic Ocean. *J Phys Oceanogr* 40(11):2496–2510
- Gillett NP, Stone DA, Stott PA, Nozawa T, Karpechko AY, Hegerl GC, Wehner MF, Jones PD (2008) Attribution of polar warming to human influence. *Nat Geosci* 1(11):750–754
- Glessmer MS, Eldevik T, Våge K, Nilsen JEØ, Behrens E (2014) Atlantic origin of observed and modelled freshwater anomalies in the Nordic seas. *Nat Geosci* 7:801–805
- Goosse H, Holland MM (2005) Mechanisms of decadal Arctic climate variability in the Community Climate System Model, version 2 (CCSM2). *J Clim* 18(17):3552–3570
- Jungclaus JH, Koenigk T (2010) Low-frequency variability of the Arctic climate: the role of oceanic and atmospheric heat transport variations. *Clim Dyn* 34(2–3):265–279
- Levitus S, Matishov G, Seidov D, Smolyar I (2009) Barents Sea multidecadal variability. *Geophys Res Lett* 36(19):L19604
- Mahajan S, Zhang R, Delworth TL (2011) Impact of the Atlantic Meridional Overturning Circulation (AMOC) on arctic surface air temperature and sea ice variability. *J Clim* 24(24):6573–6581
- Marsland S, Bi D, Uotila P, Fiedler R, Griffies S, Lorbacher K, O’Farrell S, Sullivan A, Uhe P, Zhou X et al (2013) Evaluation of ACCESS climate model ocean diagnostics in CMIP5 simulations. *Aust Meteorol Oceanogr* J 63(1):101–119
- Massonnet F, Fichefet T, Goosse H, Bitz CM, Philippon-Berthier G, Holland MM, Barriat PY (2012) Constraining projections of summer Arctic sea ice. *Cryosphere* 6(6):1383–1394
- Miles MW, Divine DV, Furevik T, Jansen E, Moros M, Ogilvie AE (2014) A signal of persistent Atlantic multidecadal variability in Arctic sea ice. *Geophys Res Lett* 41(2):463–469
- Parker D, Folland C, Scaife A, Knight J, Colman A, Baines P, Dong B (2007) Decadal to multidecadal variability and the climate change background. *J Geophys Res Atmos* 112:D18115
- Polyakov I, Alekseev G, Timokhov L, Bhatt U, Colony R, Simmons H, Walsh D, Walsh J, Zakharov V (2004) Variability of the Intermediate Atlantic Water of the Arctic Ocean over the last 100 years. *J Clim* 17(23):4485–4497

- Polyakov IV, Bekryaev RV, Alekseev GV, Bhatt US, Colony RL, Johnson MA, Maskhtas AP, Walsh D (2003) Variability and trends of air temperature and pressure in the maritime Arctic, 1875–2000. *J Clim* 16(12):2067–2077
- Proshutinsky AY, Johnson MA (1997) Two circulation regimes of the wind-driven Arctic ocean. *J Geophys Res Oceans* 102(C6):12,493–12,514
- Serreze MC, Barry RG (2011) Processes and impacts of Arctic amplification: a research synthesis. *Glob Planet Change* 77(1):85–96
- Serreze MC, Barrett AP, Slater AG, Steele M, Zhang J, Trenberth KE (2007) The large-scale energy budget of the Arctic. *J Geophys Res Atmos* 112:D11122
- Shaffrey L, Sutton R (2006) Bjerknæs compensation and the decadal variability of the energy transports in a coupled climate model. *J Clim* 19(7):1167–1181
- Smedsrud LH, Esau I, Ingvaldsen RB, Eldevik T, Haugan PM, Li C, Lien VS, Olsen A, Omar AM, Otterå OH et al (2013) The role of the Barents Sea in the Arctic climate system. *Rev Geophys* 51(3):415–449
- Stroeve JC, Kattsov V, Barrett A, Serreze M, Pavlova T, Holland M, Meier WN (2012) Trends in Arctic sea ice extent from CMIP5, CMIP3 and observations. *Geophys Res Lett* 39(16):L16502
- Van der Swaluw E, Drijfhout S, Hazeleger W (2007) Bjerknæs compensation at high northern latitudes: the ocean forcing the atmosphere. *J Clim* 20(24):6023–6032
- Taylor KE, Stouffer RJ, Meehl GA (2012) An overview of CMIP5 and the experiment design. *Bull Am Meteorol Soc* 93(4):485–498
- Wouters B, Drijfhout S, Hazeleger W (2012) Interdecadal North-Atlantic meridional overturning circulation variability in EC-EARTH. *Clim Dyn* 39(11):2695–2712